Journal of Nuclear Materials 389 (2009) 173–178

Contents lists available at ScienceDirect

Journal of Nuclear Materials

journal homepage: www.elsevier.com/locate/jnucmat

Evaluation of phosphate thermodynamic properties for spent electrolyte recycle

Hirohide Kofuji [a,b,*], Ippei Amamoto [a], Masaru Yasumoto [b], Kazuya Sasaki [b], Munetaka Myochin [a], Takayuki Terai [b]

[a] Pyrochemical Reprocessing Gr., Japan Atomic Energy Agency, Tokai, Ibaraki 319-1194, Japan
[b] The School of Engineering, The University of Tokyo, Bunkyo, Tokyo 113-8656, Japan

A B S T R A C T

Adaptation of the phosphate conversion technique was undertaken and evaluated for application to the recycle process of the spent electrolyte generated from metal electrorefining process. In order to confirm the conversion behaviors of fission product (FP) chlorides to the phosphates, conversion experiments were carried out for some alkali metal, alkaline earth metals and rare-earth elements and their results were compared with that of thermodynamic calculations of previous study [I. Amamoto, H. Kofuji, M. Myochin et al., in: Proceedings of Global 2007, Boisi, Idaho, USA, 2007]. Among these elements, rare-earth chlorides were converted into phosphates and Cs was not, according to the prediction by the calculation. As for alkaline earth metals, their equilibrium constants were nearly 1 based on the results of the calculations, the conversion reactions were difficult to occur. In addition, it was clarified that phosphates were thermally unstable, easily to decompose at higher temperature, through the measurements of their heat flow and vapor pressure.

1. Introduction

In the metal electrorefining process which is one of the pyrochemical reprocessing methods, the nuclear materials such as uranium (U) and transuranic elements (TRU) are recovered from molten salt through electrolytic operation using solid and liquid metal electrodes [2,3]. The electrolyte used for eutectic medium will be contaminated by accumulation of various actinide (Ac) and fission product (FP) elements after prolonged electrolysis operation. This seems to cause the rising of the melting point of the molten salt and lowering of the current efficiency. Accordingly, it is necessary to replace the electrolyte contaminated with FP elements periodically to keep the electrolyte satisfactory condition, however it causes generation of enormous volume of high-level radioactive waste (HLW) because the spent electrolyte is classified as HLW. For the reduction of the amount of HLW, recycling use of electrolyte is required by removing the FP elements and minor actinide (MA) from it.

One of the treatment methods of spent electrolyte, phosphate conversion technique has been developed at Research Institute of Atomic Reactor (RIAR) in Russia [4]. In the RIAR method, contaminant such as MA and rare-earth elements (REE) are removed from NaCl–2CsCl spent electrolyte before its disposal. Although RIAR has proven its conceptual validity, further investigation is required to apply it to 3LiCl–2KCl spent electrolyte due to the differences in their chemical composition, operational temperature, etc.

The conceptual block flow diagram was proposed for the phosphate conversion technique, and consequently applicability to the 3LiCl–2KCl spent electrolyte has been evaluated [1]. The process, as shown in Fig. 1, consists of three steps, i.e., 'spent electrolyte regeneration step', 'phosphate conversion step', 'phosphate immobilization step'. It is expected that finally produced vitrified waste could contain FP elements tens of percentage of its volume according to past experimental results [5], and lead to the large reduction of the amount of HLW.

Among these three steps, conversion reaction at the spent electrolyte regeneration step was preliminary evaluated based on the thermodynamic calculation in previous study [1] because how to convert FP chloride to FP phosphate, i.e., Eq. (1), influences the feasibility of a whole process.

$$FPCl_z + (z/3)Li_3PO_4 \leftrightarrows FP(PO_4)_{z/3} + zLiCl \quad (\text{in LiCl—KCl eutectic}). \tag{1}$$

However, few data have been published relating to the thermodynamic property for phosphate, therefore, the thermodynamic data of phosphate, $\Delta_f G^\circ$ for instance, were assumed by CALPHAD (calculation of phase diagram) [6] method.

Equilibrium constants of the conversion reactions shown in Eq. (1) were individually calculated for several kinds of FP elements such as REE, alkali metals and alkaline earth metals at the range

* Corresponding author. Address: Pyrochemical Reprocessing Gr., Japan Atomic Energy Agency, Tokai, Ibaraki 319-1194, Japan. Tel.: +81 29 282 1111; fax: +81 29 282 9257.
E-mail address: kofuji.hirohide@jaea.go.jp (H. Kofuji).

0022-3115/$ - see front matter © 2009 Elsevier B.V. All rights reserved.
doi:10.1016/j.jnucmat.2009.01.025

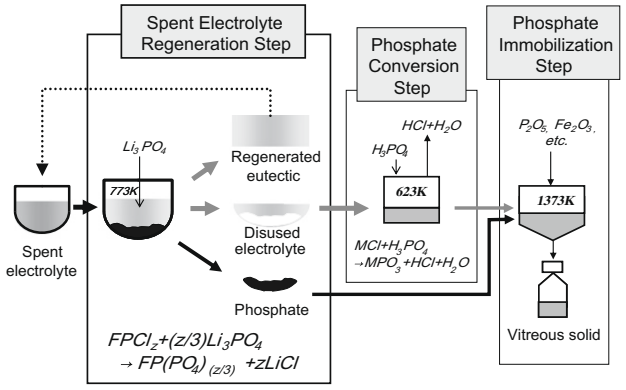

Fig. 1. Conceptual flow diagram of phosphate conversion process [1].

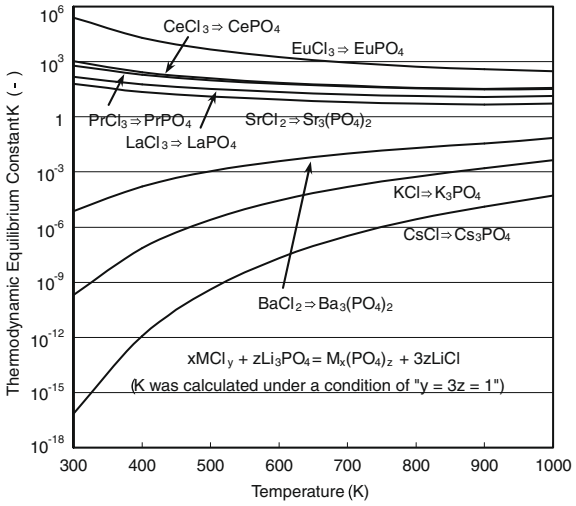

Fig. 2. Calculated equilibrium constant K for phosphate conversion reaction [1].

from 300 to 1000 K. As shown in Fig. 2, REE and Sr were assumed to be relatively easy to convert into phosphates from the results of the calculations [1].

In this study, several conversion experiments were carried out to confirm the conversion behaviours of major FP chlorides, and the behaviours were compared with the results of equilibrium calculations. The estimation of the conversion reaction, is it progressing or not, was undertaken by SEM/EDS (scanning electron microscope/embedded energy dispersive X-ray analyzer) analysis because the crystalline form of the products were important for the future study to separate phosphate by the filtration.

Furthermore, thermodynamic behaviours of Li_3PO_4 and K_3PO_4 which were the additives for conversion reactions seemed to be significant for the evaluation of conversion reactions. Therefore some measurements were carried out to understand the thermodynamic behaviours of them at high temperature using TG–DTA (thermogravimetry–differential thermal analyzer) and HTMS (high temperature mass spectrometry).

2. Experimental

2.1. Phosphate conversion reaction

The experimental operations were undertaken in the glove box with Ar atmosphere to avoid the absorption of moisture to LiCl–KCl eutectic and other materials.

Table 1
Amount of added reagent (FP chlorides and Li_3PO_4).

Impurity	Added mass		Li_3PO_4 (g)
$LaCl_3$	5 mmol	1.226 g	1.158
$CeCl_3$	5 mmol	1.232 g	1.158
$PrCl_3$	5 mmol	1.236 g	1.158
$EuCl_3$	5 mmol	1.292 g	1.158
YCl_3	5 mmol	0.976 g	1.158
CsCl	10 mmol	1.329 g	0.772
$SrCl_2$	5 mmol	0.793 g	0.772
$BaCl_2$	5 mmol	1.041 g	0.772

A kind of FP chloride, Li_3PO_4 as the additive and LiCl–KCl eutectic (10 g) were taken into an alumina crucible. It was heated up to 773 K and kept at that temperature for 2 h. As the FP chlorides, $LaCl_3$, $CeCl_3$, $PrCl_3$, $EuCl_3$, YCl_3, CsCl, $SrCl_2$ and $BaCl_2$ were examined. Added mass of each FP chloride and Li_3PO_4 are shown in Table 1. The crucibles were cooled naturally leaving sitting after the reaction had finished, then they were cut with diamond cutter and the cross-section was ground. To remove the cutting oil, cut sample was washed with the absolute ethanol by ultrasonic cleaner. The cross-section lost its lustre during washing. A SEM/EDS JSM-6390LA (JOEL Co.) was used for the microscopic observation and the elemental analysis of the cross-section.

2.2. Phase transition temperature

As the additive for conversion reaction, Li_3PO_4, K_3PO_4 and their mixture were measured their phase transition temperatures by TG-DTA (TG8120, Rigaku Co.).

For the preparation of measured sample, Li_3PO_4 (98.2%, Wako pure chemical industries) and K_3PO_4 (100%, Sigma–Aldrich) were used after drying at 383 K for 4h. All the reagents were handled in the Ar glove box. The mixtures of Li_3PO_4 and K_3PO_4 were melt blended in the platinum crucible at 1373–1523 K for 4–7 h. The mole ratios of the mixtures were determined by the ratio of Li and K concentration measured with ICP–AES OPTIMA3000 (Perkin-Elmer, Inc.). The weights of measured samples and their mole ratio (mole fraction of Li_3PO_4) were shown in Table 2. A platinum pan (5 mm diameter and 2.5 mm height) was used for TG–DTA analysis in the Ar atmosphere. The range of temperature was from room temperature to 1723 K and its programming rate was 5 K/min.

2.3. Vapour pressure

Vapour pressure of Li_3PO_4 was measured to evaluate its thermodynamic behaviour at high temperature by HTMS (12-90HT, Nuclide Co.). The device was modified to introduce various gases into the Knudsen cell and to mount a pulse counting system. Setup of the device for the vapour pressure measurement is shown in Fig. 3.

The partial vapour pressure P_i of a vapour species i in the Knudsen cell was calculated based on the following Eq. (2) [7,8].

$$P_i = kI_iT/(\sigma_i\gamma_i) \quad (2)$$

where, I_i is the ion current, σ_i is the ionization cross-section, γ_i is the isotopic abundance of species i. The quantity k is the apparatus constant.

The ion current I_i in Eq. (2) is

Table 2
Weight of samples and their mole ratio (TG–DTA).

Li_3PO_4 mole fraction (%)	0	25	50	76	100
Weight (mg)	10.84	11.53	10.47	12.10	11.18

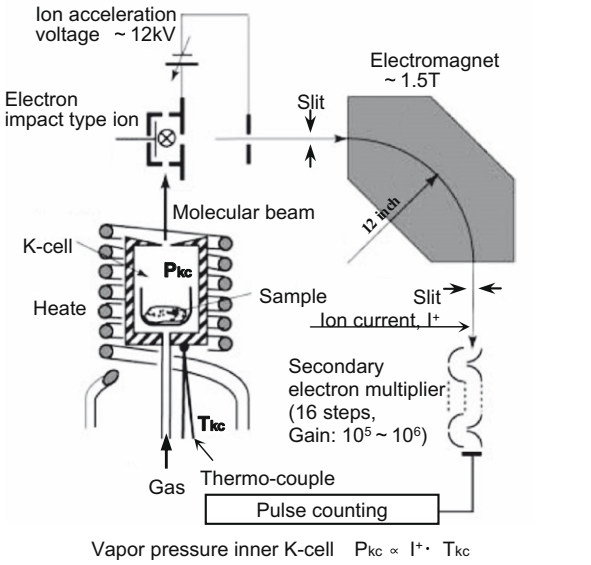

Fig. 3. Setup of high temperature mass spectrometer (HTMS).

$$I_i = rq_e/(\eta_d\eta_I) \quad (3)$$

where, r is counting rate (cps), q_e is charge of electron, η_d is multiplier gain, η_I is the correction factor of counting loss by pile-up.

In this study, vapour pressures of all ion species detected were described with I_iT because the ionization cross-section σ_i of Li_3PO_4 was unknown, therefore, an absolute value of vapor pressure could not be calculated. The orifice diameter of the platinum Knudsen cell was 0.3 mm at the initial condition (it had been expanded to 0.8 mm later). Before the measurement, apparatus constant k was determined by the measurement of Ag whose vapor pressure and ionization cross-section are well known. About 100 mg of Li_3PO_4 (98.2%; Wako pure chemical industries) was loaded into the Knudsen cell after drying 4 h at 383 K. Subsequently, loaded sample was annealed 6 h at 873 K to remove LiOH and Li_2CO_3 which were assumed impurities originally involved in the reagent or generated at experimental process. The range of the measurement temperature was 1273–1623 K which was around the melting point of Li_3PO_4 (1478 K) [9].

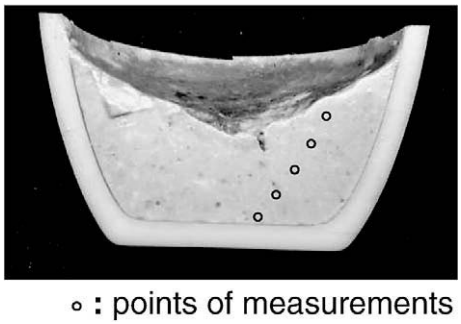

Fig. 4. An example of cross-section of observed sample (LiCl–KCl–YCl_3–Li_3PO_4).

3. Results and discussion

3.1. Phosphate conversion reaction

The thermodynamic calculations were carried out in the previous study by FactSage, integrated thermodynamic databank system by GTT Technologies Ltd. [6]. The conversion reaction of FP chlorides into phosphates in LiCl–KCl eutectic were described by the thermodynamic equilibrium constant K calculated based on the Eqs. (4) and (5) when the formula shown in Eq. (1) maintained the thermodynamic equilibrium condition.

$$RT\ln K = -\Delta_r G^\circ \quad (4)$$

$$\Delta_r G^\circ = \sum_j \nu_j \Delta_f G^\circ(j) \quad (5)$$

where, R is gas constant [8.31451 JK^{-1} mol^{-1}], T is temperature (K), ν is stoichiometric coefficient and $\Delta_r G^\circ$ is the standard reaction Gibbs function. For the calculation, $\Delta_f G^\circ$ (kJ mol^{-1}) for the standard

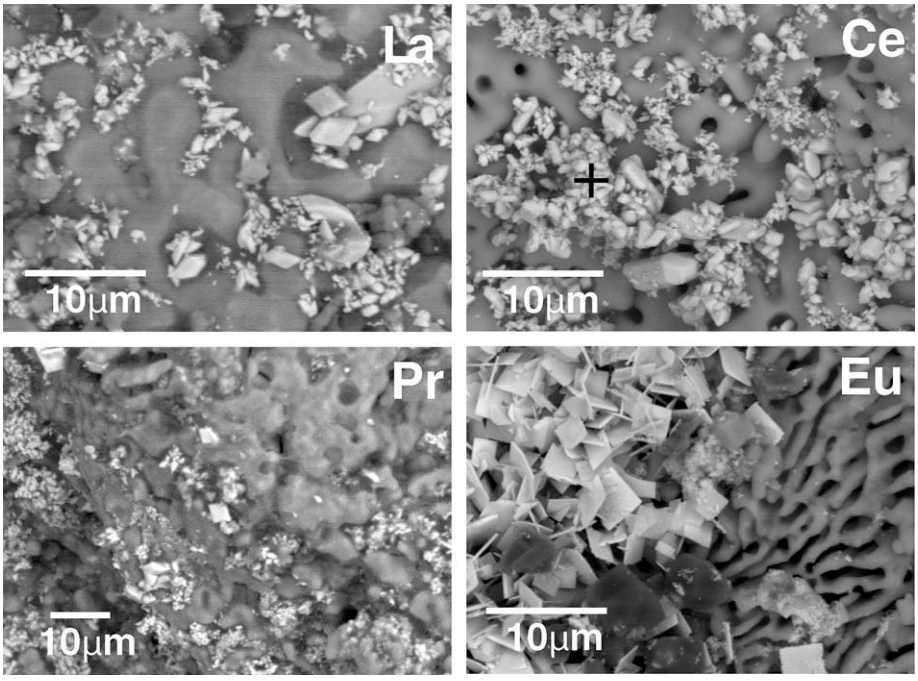

Fig. 5. SEM images of conversion products (lanthanoids).

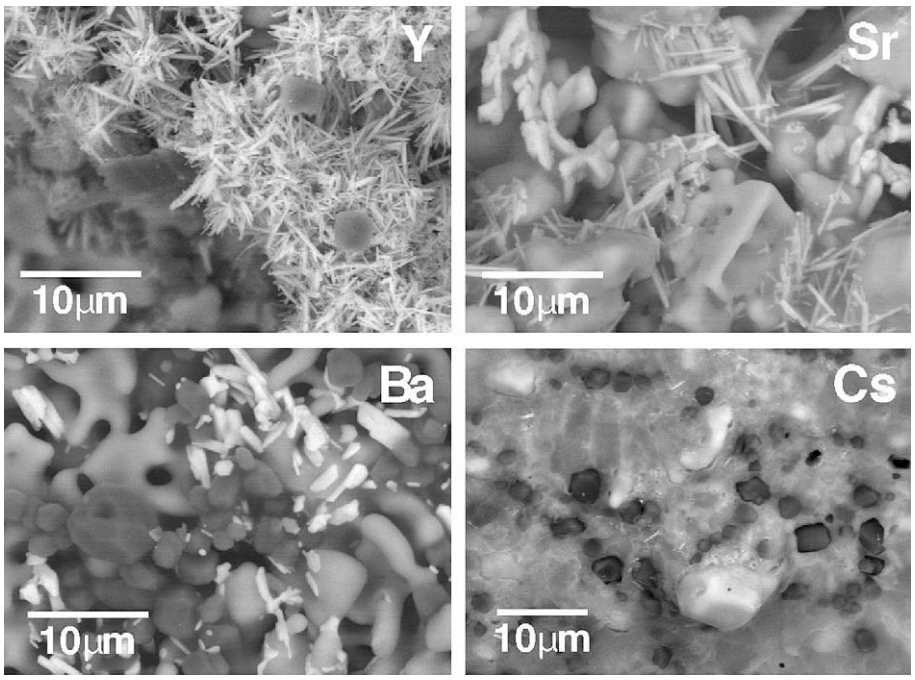

Fig. 6. SEM images of cross-section around the bottom areas (Y, Sr, Ba and Cs).

Gibbs function of FP phosphates were employed from the computational results by CALPHAD method. The activity coefficient γ had not been known, such presumption was taken that all γ would be nearly 1 [10].

Fig. 2 shows the results of the calculation of K at the temperature range of 300–1000 K. In the case that Li_3PO_4 was added, the selected REE and Sr chlorides were assumed to be possible to convert into phosphates at all temperature range of K calculated. On the other hand, Ba, Cs and K chlorides were not assumed to convert into phosphates.

The FP chlorides shown in Table 1 were tested their conversion reaction to the phosphates individually in this study. The diverting agent was Li_3PO_4. Fig. 4 shows the example of the cross-section of the sample. SEM images of the samples are shown in Fig. 5 for lanthanoids (Ln), and in Fig. 6 for Y, Sr, Ba and Cs. SEM observations were mainly carried out around bottom area of the crucible.

The crystal observed in the samples of La, Ce, Pr, Eu and Y were suggested to be the converted phosphate because P, O and metal elements were detected by the EDS analyses. For example, the spectrum of EDS at the point of the crystal observed in the sample of Ce, marked '+' in Fig. 5, was shown in Fig. 7. This was a typical pattern of EDS signal of the FP phosphate measured in this study.

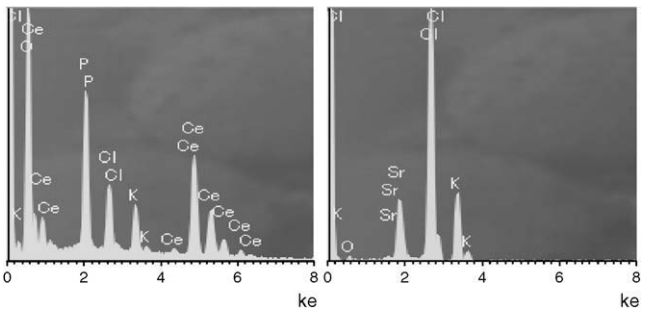

Fig. 7. An example of EDS signal for FP phosphate (Ce phosphate, near the bottom of the crucible).

The crystals of other samples indicated almost the same spectra. Only K and Cl were detected in the areas of the background of the crystal. Therefore, they were assumed to be LiCl–KCl because Li was insensible in EDS. Furthermore, these crystals were observed mainly at the bottom areas and rarely observed in the upper side of the crucible.

As for the sample of Ba, a little of crystal of Ba phosphate was observed as shown in Fig. 6. Though some crystal was also found in the SEM image of Sr sample, it was determined to be $SrCl_2$ by EDS (see Fig. 7). As well as the Cs sample, definitely crystal of phosphate was not found.

From the results of these conversion experiments, the conversion behaviours of REE appear to be in agreement with the results of the thermodynamic calculations. This suggests the possibility of the separation of FP elements by using suitable filter which has the tolerance of high temperature because the melting points of Ln orthophosphates, more than 2000 K [11], are much higher than that of the melt.

The alkaline earth metals, i.e., Sr and Ba, indicated the different tendency from the results of the calculation. $SrCl_2$ was expected to convert to phosphate judging from the thermodynamic calculation, however, the conversion reaction was not proceeded in this experiment. A little of Ba phosphate, conversion product, was found near the bottom of the crucible (see Fig. 6), and this didn't agree with the thermodynamic calculation.

According to the comparison of both results of thermodynamic calculations and conversion tests, it could not be expected that the conversion reaction proceeded near the range of '$K = 1$' in the calculation. It seemed that such an uncertainty was caused from the error of assumed $\Delta_f G^\circ$ and γ.

3.2. Phase transition temperature of Li_3PO_4 and K_3PO_4

Fig. 8 shows the measured DTA. The baseline was not steady in any data. The heat flow of Li_3PO_4 was particularly shifted, its baseline was corrected by fitting to polynomial approximation. The phase transition temperatures of Li_3PO_4–K_3PO_4 binary system were assumed from these endothermic signals shown in Table 3.

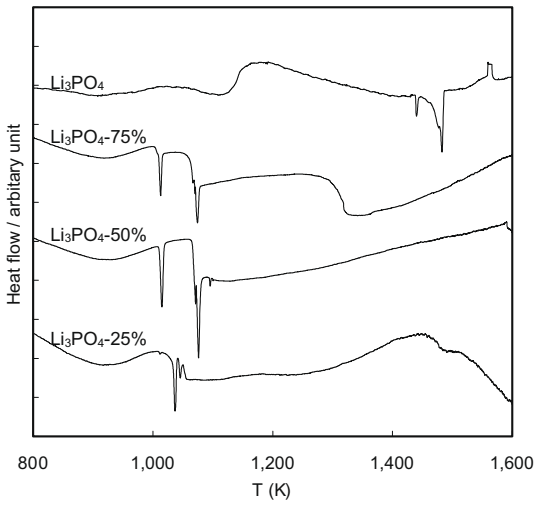

Fig. 8. DTA charts of Li_3PO_4 and Li_3PO_4–K_3PO_4.

Table 3
Phase transition temperature and melting point estimated from endothermic peak of DTA.

Li_3PO_4 mole fraction (%)	Phase transition temperature (K)			Liquidus temperature (K)
25	1010	1044	1457	1457
50	1011	1066	–	1066
76	1010	1063	1317	1317
100	1438	1480	–	1480

However, the peak signals of 0.25 Li_3PO_4–0.75 K_3PO_4 at around 1010 and 1457 K were extremely weak.

The liquidus curve and the eutectic line were drawn based on these DTA data and the published melting point of pure substances (see Fig. 9). The eutectic temperature of Li_3PO_4–K_3PO_4 system was assumed to be around 1065 K and eutectic composition was about 50 mol% of Li_3PO_4 content. The endothermic peaks observed at 1010 and 1011 K seemed to depend on some phase transition in the solid phase. However, the assumed phase transition temperatures were considered to involve some error margins because Li_3PO_4 and K_3PO_4 were thermally unstable from the results of these measurements.

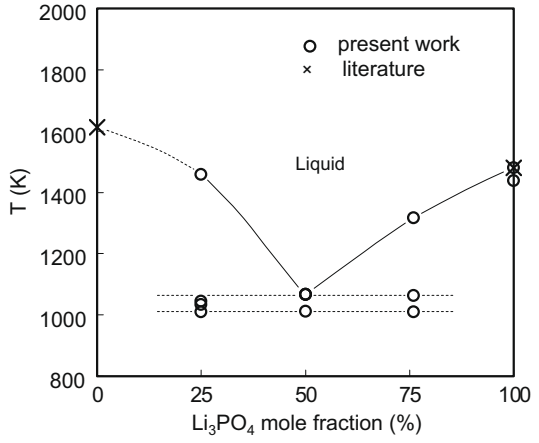

Fig. 9. Estimated phase diagram for Li_3PO_4–K_3PO_4.

3.3. Vaporization property of Li_3PO_4 (HTMS)

At the first measurement of Li_3PO_4 as a pure substance, Li, Li_3PO_4, $LiPO_3$, PO_2 and O_2 were detected as the vapor species using the Knudsen cell with an orifice of 0.3 mm in diameter. These vapor species except Li_3PO_4 were confirmed not to be originated from fragmentation of Li_3PO_4. Furthermore, it was thought that $LiPO_3$ showed a high vapor pressure even if its content was very low because it was not detected by XRD in the sample after measurement.

The relationships between ion current and temperature of Li, Li_3PO_4 and $LiPO_3$ were shown in Fig. 10. It was generally known that the natural logarithm of the vapor pressure and the inverse of the temperature were linier relationship by the Clausius-Clapeyron equation as shown in Eq. (6) [10].

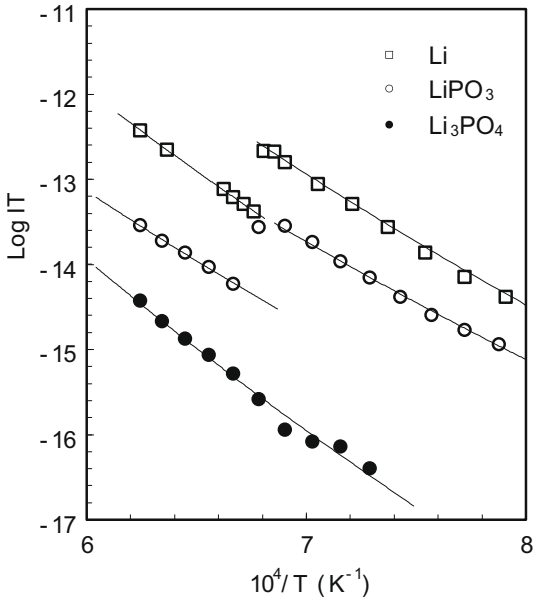

Fig. 10. Ion current of Li, $LiPO_3$ and Li_3PO_4 (first measurement, sample: Li_3PO_4).

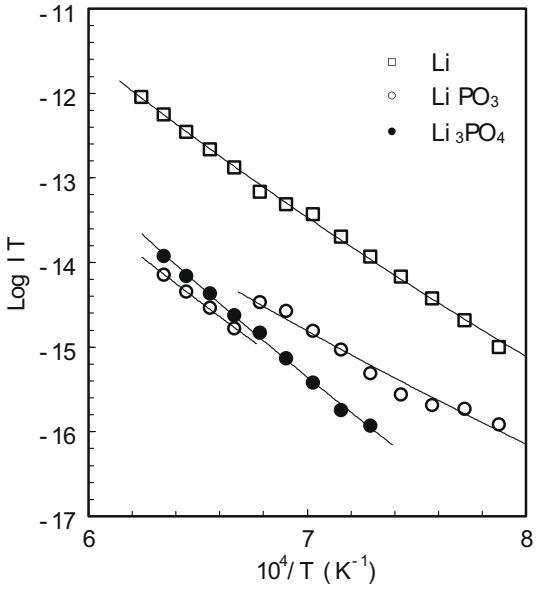

Fig. 11. Ion current of Li, $LiPO_3$ and Li_3PO_4 (improved measurement, sample: Li_3PO_4).

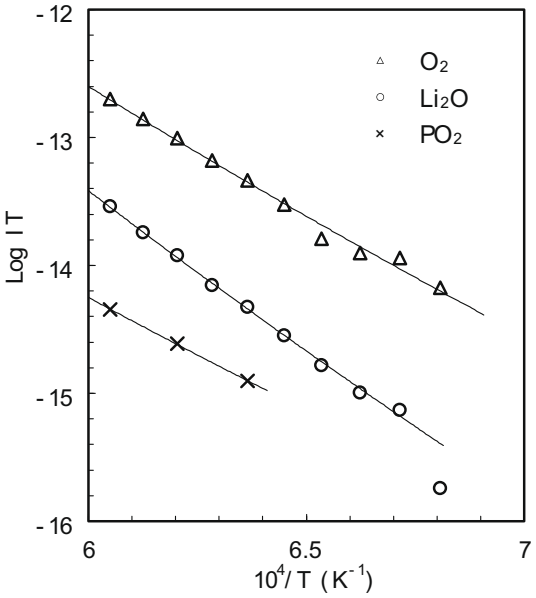

Fig. 12. Ion current of O_2, Li_2O and PO_2 (improved measurement, sample: Li_3PO_4).

$$\ln P = -\frac{\Delta H_{vap}}{RT} + C \tag{6}$$

where, P is the equilibrium vapor pressure, ΔH_{vap} is the molar enthalpy of vaporization and C is a constant of integration.

Though the I_iT of Li, Li_3PO_4 and $LiPO_3$ in this study and T^{-1} indicated linear relationship, there were the discontinuities in I_iT of Li and $LiPO_3$ near the melting point of Li_3PO_4.

The results of improved measurements are shown in Fig. 11. To promote the removal of $LiPO_3$ from the cell, following improvements were attempted. The annealing temperature and time were raised to 1373 K and lengthened to 10 h. In addition, the diameter of the orifice was expanded to 0.8 mm. The ion current of $LiPO_3$ was considerably reduced by these improvements, however, Li_2O was newly detected seen in Fig. 12. This is thought to be generated by thermal decomposition reaction of Eq. (7).

$$Li_3PO_4 \rightarrow LiPO_3 + Li_2O. \tag{7}$$

In all measurements of this study, the vapor pressure of Li were extremely high even if a further decomposition of Eq. (7) was premised, thus it was assumed that the decomposition products diffused slowly in the solid phase and surface of the sample had not been in the equilibrium between solid and vapor phase.

4. Conclusions

The REE chlorides were confirmed experimentally to be converted to the phosphates in the molten LiCl–KCl by addition of Li_3PO_4. These suggest the possibility of the removal of the FP elements from the spent electrolyte by use of appropriate filter medium. On the other hand, the conversion reaction of CsCl has not progressed and it was the same tendencies as the results of the thermodynamic calculations. As for $SrCl_2$ and $BaCl_2$, their equilibrium constants were nearly 1, the results of the reaction were different from that assumed by the thermodynamics calculation. The error was thought to occur on account of the assumed $\Delta_f G^\circ$ of the phosphates and the assumption of activity coefficient, $\gamma = 1$. Thus, a little error of the thermodynamic data influences whether the reaction is progressed or not in the case of the equilibrium constant K is nearly 1.

Accordingly, accurate thermodynamic data were required for the phosphate to estimate the phosphate conversion reaction. The thermodynamic behaviour of Li_3PO_4 and K_3PO_4 were evaluated as an example, it was clarified that phosphates were thermally unstable, decomposed easily, due to its properties obtained through TG–DTA and HTMS measurements. Therefore, assumed phase diagram of Li_3PO_4–K_3PO_4 in this study was thought to be accompanied with some uncertainty.

References

[1] I. Amamoto, H. Kofuji, M. Myochin et al., in: Proceedings of Global 2007, Boisi, Idaho, USA, 2007.
[2] J.J. Laidler, J.E. Battles, W.E. Miller et al., in: Proceedings of Global 93, Seattle, WA, USA, September 12–17, 1993, p. 1061.
[3] L. Burris, R.K. Steunenberg, W.E. Miller, in: Proceedings of Annual AICHE Meeting, Miami, FL, November 2–7, 1986, p. 135.
[4] A.A. Minaev, A.K. Pikaev, D.G. Kuznetsov et al., in: Proceedings of ATALANTE 2004 Advances for Future Nuclear Fuel Cycle, Nimes, France, June 21–24, 2004, p. 4–18.
[5] M. Sazarashi, K. Maruyama, S. Ono et al., in: Proceedings of Global 2003, New Orleans, LA, November 16–20, 2003, p. 1107.
[6] C.W. Bale, P. Chartrand, S.A. Degterov et al., Calphad 26 (2) (2002) 189.
[7] M. Asano, H. Nakagawa, J. Nucl. Mater. 160 (1988) 172.
[8] T. Koyama, M. Yamawaki, J. Nucl. Mater. 152 (1988) 30.
[9] D.R. Lide, CRC Handbook of Chemistry and Physics, CRC, Boca Raton, USA, 2004. p. 4-66.
[10] P.W. Atkins, J. de Paula, ATKINS' Physical Chemistry, 8th Ed., Oxford UP, Oxford, UK, 2006. p. 128.
[11] Y. Hikichi, T. Nomura, J. Am. Ceram. Soc. 70 (10) (1987) C252.